A Theory for the Proton Transport of the Influenza Virus M2 Protein: Extensive Test against Conductance Data

Huan-Xiang Zhou*
Department of Physics and Institute of Molecular Biophysics, Florida State University, Tallahassee, Florida

ABSTRACT A theory for calculating the proton flux through the influenza virus M2 channel is tested here against an extensive set of conductance data. The flux is determined by the rate constants for binding to the His^{37} tetrad from the two sides of the membrane and the corresponding unbinding rate constants. The rate constants are calculated by explicitly treating the structure and dynamics of the protein. Important features revealed by previous studies, such as a gating role for Val^{27} at the entrance to the channel pore, and channel activation by viral exterior pH, are incorporated in this theory. This study demonstrates that the conductance function of the M2 proton channel can now be quantitatively rationalized by the structure and dynamics of the protein.

INTRODUCTION

One of the coat proteins of the influenza A virus, M2, is a proton channel (1,2). This channel activity is essential for viral replication (3). M2 functions as a tetramer; each monomer has a single transmembrane helix. The pore for proton transport is formed at the center of the transmembrane helix bundle, with the N-terminals facing the viral exterior and the C-terminals facing the viral core. The channel is activated by the low pH of the endosome while the virion is encapsulated there. Proton transport through the M2 protein acidifies the viral core, facilitating the release of viral RNA to the host cell. The structure, dynamics, and function of the M2 proton channel have been the focus of intense studies (4–19). These studies have set the stage for correlating channel function with protein structure and dynamics. Toward that goal, a microscopic theory that accounts for the structure and dynamics of the M2 protein was developed to calculate the proton flux (20). Qualitatively, the theory was promising in that it captured the main characteristics of the M2 conductance activity. In this article, we show that the theory is able to quantitatively reproduce an extensive set of conductance data (7,12,16).

In our theory, the motions of permeant protons are modeled as diffusive (see Fig. 1). It should be noted that the mechanism for proton movement through water involves shuttling along a water chain: an excess proton transiently associates with a water molecule to form a hydronium ion; a proton then hops from the hydronium ion to the next water molecule to form another hydronium ion (21). This Grotthuss mechanism differs from the hydrodynamic diffusion of other ions, and explains why the apparent diffusion constant, D, of the proton, 10^3 Å^2/ns (22), is around fivefold higher than those of other univalent ions of similar size. As noted previously (20), this diffusion constant can explain the high rate constant, 10^{10} M^{-1} s^{-1}, of proton binding to an imidazole in aqueous solution (23), assuming that the binding is diffusion-limited. To pass through the M2 channel pore, we suppose that a permeant proton first binds to and then unbinds from an internal site, i.e., the His^{37} tetrad. This obligatory binding site has strong experimental support (17,18). Furthermore, the motion of the permeant proton through the pore is gated by Val^{27} on the N-terminal side and by Trp^{41} on the C-terminal side. The gating role of Trp^{41} has long been recognized (15). More recently, based on molecular dynamics (MD) simulations, Val^{27} has been proposed as a secondary gate (9). Although the gating dynamics of Val^{27} is assumed to be local, the gating dynamics of Trp^{41} is assumed to be coupled to the backbone dynamics of the transmembrane domain (11).

The transport of a proton through the M2 channel starts from the bulk solution in the viral exterior. The proton enters the pore by diffusion, passes through the Val^{27} gate when it is open, and diffuses further down the pore to bind to the (doubly protonated (18)) His^{37} tetrad. The bound proton is then released to either the N-terminal pore or, provided the Trp^{41} gate is open, the C-terminal pore. In the latter case, the proton diffuses out to the bulk solution in the viral core and completes the transport process. This process can also be reversed, bringing one proton from the viral core to the exterior bulk solution. Let the diffusion-influenced rate constants for proton binding to the internal site from the viral exterior and interior be k_{e+} and k_{i+}, respectively, and the rate constants for releasing a bound proton to the viral exterior and interior be k_{e-} and k_{i-}, respectively. When the proton concentrations in the viral exterior and interior are C_e and C_i, respectively, the net proton influx is

$$I = \frac{-k_{e+}k_{i-}C_e + k_{i+}k_{e-}C_i}{k_{e-} + k_{i-} + k_{e+}C_e + k_{i+}C_i}. \quad (1)$$

Submitted June 15, 2010, and accepted for publication January 4, 2011.

*Correspondence: hzhou4@fsu.edu

Editor: Nathan Andrew Baker.

0006-3495/11/02/0912/10 $2.00

doi: 10.1016/j.bpj.2011.01.002

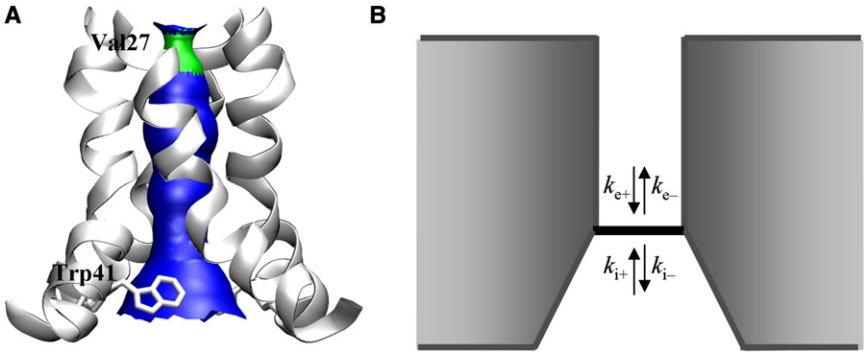

FIGURE 1 Structure of the M2 transmembrane domain and model for calculating the proton flux. (*A*) The open conformation, in which the Trp^{41} gate is swung to the side to allow proton binding from the C-terminal side. Note that the Val^{27} gate at the N-terminal pore entrance is still closed; its transient opening allows proton binding from the N-terminal side. The conformation is taken from Yi et al. (11). (*B*) Idealized geometry used for flux calculation. In the full model, a fluctuating gate is present at the N-terminal pore entrance and the C-terminal pore interconverts between the open conformation illustrated here and a closed conformation.

In terms of the exterior pH, one may write $C_e = 10^{-pHe}$; in a similar way, $C_i = 10^{-pHi}$.

Equation 1 is derived from a set of steady-state rate equations. In previous rate-equation based models of ion transport, the rate constants are simply taken as adjustable parameters (24–26). Our theory goes one step further: we calculate the rate constants of Eq. 1 by treating the diffusional motion of the permeant ion and the gating motions of the channel protein. Thus, we directly incorporate the structure and dynamics of the M2 channel into our theory. Note that in our treatment, the ion-transport system is now represented at the same level as in the Poisson-Nernst-Planck theory (25,27,28). However, our theory is distinct from the Poisson-Nernst-Planck theory in two respects. In the latter theory, one calculates the ion flux from the steady-state electrodiffusion gradient. The channel pore in our theory explicitly contains an obligatory binding site for the permeant ion, and we calculate the rate constants, k_{e+} and k_{i+}, for the permeant ion binding to this internal site from the two sides of the membrane. More importantly, our channel is not static but dynamic, and we explicitly account for the effects of the gating motions of the channel on k_{e+} and k_{i+}. Note that k_{e+} or k_{i+} is an effective rate constant involving the whole process of a proton starting in the bulk solution, diffusing into the dynamic channel and to the internal site, and finally binding to it. The last step is assumed to be fast (corresponding to an absorbing boundary condition), and hence, the overall binding rate constant is diffusion-controlled.

Equation 1 predicts that the proton influx exhibits a sharp increase when pH_e is lowered to the third pK_a of the His^{37} tetrad, which is 6.3 ± 0.3 (18). Because of the asymmetry in geometry and in gating dynamics between the N-terminal pore and the C-terminal pore (see Fig. 1), k_{e+} and k_{i+} have different values; correspondingly, k_{e-} and k_{i-} are also different. As a result, the influx and efflux are predicted to be asymmetric when the pH gradient across the membrane is reversed. All of these are qualitative features observed in M2 conductance measurements (12,16). Here, we extend and refine our theory for proton transport and show that it is capable of quantitatively reproducing a significant amount of experimental conductance data.

THEORY

Here, we outline the basic theory for calculating the diffusion-controlled binding rate constants k_{e+} and k_{i+}. In most of the experiments, a voltage was applied across the membrane. We describe below how a transmembrane voltage is accounted for. The M2 proton channel is activated by low pH_e. The activation is explicitly modeled here.

Relation between binding and unbinding rate constants

The unbinding rate constants, k_{e-} and k_{i-}, are related to the corresponding binding rate constants, k_{e+} and k_{i+}, through the dissociation constants, K_{de} and K_{di}. If there is no change in chemical potential when a proton is transferred from the bulk solution on either side of the membrane to the internal site, then both K_{de} and K_{di} are equivalent to the third pK_a of the His^{37} tetrad, which hereafter will be denoted as pK_{a0}. In this case, we have

$$K_{de} = \frac{k_{e-}}{k_{e+}} = 10^{-pK_{a0}}, \tag{2a}$$

$$K_{di} = \frac{k_{i-}}{k_{i+}} = 10^{-pK_{a0}}. \tag{2b}$$

If a transmembrane voltage is applied, then there are differences in chemical potential, to be denoted as ΔU_e and ΔU_i, respectively, between the internal site and the two bulk solutions. We now have

$$K_{de} = \frac{k_{e-}}{k_{e+}} = 10^{-pK_{a0}} e^{\Delta U_e/k_B T}, \tag{3a}$$

$$K_{di} = \frac{k_{i-}}{k_{i+}} = 10^{-pK_{a0}} e^{\Delta U_i/k_B T}, \tag{3b}$$

where k_B is Boltzmann's constant and T is the absolute temperature. These relations allow us to focus on the binding rate constants k_{e+} and k_{i+}.

Binding to the internal site in the static pore

We treat the binding to the internal site as diffusion-controlled. Therefore, the internal site, as a disk spanning the cross section

of the pore, serves as an absorbing boundary to protons coming to the pore from either side of the membrane. Though the theory allows the binding to be treated as partial absorption, it has been argued previously that proton binding to the His^{37} tetrad is diffusion-controlled and an absorbing boundary condition is appropriate for modeling the M2 proton channel (20). For now, the pore is assumed to be static, and correspondingly, the rate constants are denoted as k_{se+} and k_{si+}. Let x denote the coordinate along the pore axis, with value 0 at the entrance from the viral exterior and value L at the exit to the viral core. The pore is assumed to be axially symmetric, with radius a_e at $x = 0$ and radius a_i at $x = L$. The internal site is located at $x = L_e$. We denote the potential of mean force along the pore axis as $U(x)$, and the cross-sectional area as $\sigma(x)$. The reference of $U(x)$ is chosen such that $U(0) = 0$. The difference in potential of mean force between the two ends of the pore, $U(L) - U(0)$, is denoted as ΔU. Note that $\Delta U = \Delta U_e - \Delta U_i$. This basic model, except for the boundary condition at the internal binding site, is similar to what underlies the Poisson-Nernst-Planck theory, and is hence subject to all the caveats noted previously for the Poisson-Nernst-Planck theory (27).

The rate constants are given by (A. M. Berezhkovskii, A. Szabo, and H.-X. Zhou, unpublished)

$$\frac{1}{k_{se+}} = \frac{1}{4Da_e} + \int_0^{L_e} dx\left[D\sigma(x)e^{-U(x)/k_BT}\right]^{-1}, \tag{4a}$$

$$\frac{1}{k_{si+}} = \frac{1}{4Da_i} + \int_{L_e}^{L} dx\left[D\sigma(x)e^{-(U(x)-\Delta U)/k_BT}\right]^{-1}. \tag{4b}$$

These expressions bear resemblance to some of the results in the Poisson-Nernst-Planck theory (25). In fact, for the static pore considered at the moment, it can be shown that when the internal binding site is represented as a deep energy well, our theory gives the same result for the ion flux as does the Poisson-Nernst-Planck theory. We model the N-terminal pore as a cylinder, with radius a. The C-terminal pore is assumed to be a topless cone, with radius a at the internal binding site and radius a_e at the pore exit. When $U(x) = 0$, we find that

$$\frac{1}{k_{se+}} = \frac{1}{4Da} + \frac{L_e}{\pi Da^2}, \tag{5a}$$

$$\frac{1}{k_{si+}} = \frac{1}{4Da_i} + \frac{L_i}{\pi Da a_i}, \tag{5b}$$

where $L_i = L - L_e$. These results are found in an earlier work (20).

Effect of a transmembrane voltage

A transmembrane voltage, V, corresponds to a change of $\Delta U = eV$ in the potential of mean force, where e is the protonic charge. We assume that the change is linearly accrued along the pore, resulting in a potential of mean force (29,30)

$$U(x) = \frac{eV}{L}x. \tag{6}$$

The differences in potential between the internal site and the two bulk solutions are

$$\Delta U_e = eV\frac{L_e}{L}, \tag{7a}$$

$$\Delta U_i = -eV\frac{L_i}{L}. \tag{7b}$$

Equation 4 now becomes

$$\frac{1}{k_{se+}} = \frac{1}{4Da} + \frac{e^{\alpha}-1}{\alpha}\frac{L_e}{\pi Da^2}, \tag{8a}$$

$$\frac{1}{k_{si+}} = \frac{1}{4Da_i} + \frac{1}{\pi D}\int_0^{L_i} dx\,\frac{e^{-eVx/Lk_BT}}{\left[a_i + (a-a_i)x/L_i\right]^2}. \tag{8b}$$

Equation 8a, which introduces a symbol α to denote $\Delta U_e/k_BT$, is found in an earlier work (20). No closed-form expression for the integral in Eq. 8b is available; hence, we evaluate it here by numerical integration.

Val^{27} gating

As noted above, our channel is not static but dynamic. We model the four Val^{27} residues near the pore entrance as a gate at $x = 0$ that stochastically opens and closes. Let the open-closed transition rates be ω_o and ω_c,

$$\text{open} \underset{\omega_o}{\overset{\omega_c}{\rightleftharpoons}} \text{closed},$$

and let $\omega = \omega_o + \omega_c$. Following earlier work (31), the rate constant for binding from the viral exterior is given by

$$\frac{1}{k_{e+}} = \frac{1}{k_{se+}} + \frac{\omega_c}{\omega_o}\left[\frac{1}{\omega\hat{k}_{eB}(\omega)} + \frac{1}{\omega\hat{k}_{eP}(\omega)}\right]. \tag{9}$$

We now explain the two new quantities appearing in the brackets. $\hat{k}_{eB}(s)$ is the Laplace transform,

$$\hat{k}_{eB}(s) = \int_0^{\infty} dt e^{-st}k_{eB}(t), \tag{10}$$

of the time-dependent rate coefficient, $k_{eB}(t)$, for protons in the exterior bulk solution being absorbed at the pore entrance. The steady-state value of $k_{eB}(t)$ is $4Da$, the inverse of the first term in Eq. 5a. An accurate approximate expression for $\hat{k}_{eB}(s)$ is (32)

$$s\widehat{k}_{\mathrm{eB}}(s)/4Da = 1+(\pi/4)\left(sa^2/D\right)^{1/2} - \frac{(1-\pi/4)(sa^2/D)^{1/2}}{(1-\pi/4)\pi/2(\pi^2/8-1)+(sa^2/D)^{1/2}}. \quad (11)$$

The other quantity, $\widehat{k}_{\mathrm{eP}}(s)$, is the Laplace transform of the total flux across the N-terminal pore entrance, under the condition that the initial distribution of the proton is uniformly zero in the N-terminal pore and its distribution function at the pore entrance is maintained at 1. The boundary condition at the other end of the N-terminal pore, i.e., at the internal binding site, is absorbing. For the linear potential of Eq. 6, the result is (see Appendix A)

$$s\widehat{k}_{\mathrm{eP}}(s)/\left(\pi Da^2/L_{\mathrm{e}}\right) = \gamma\coth\gamma - \alpha/2, \quad (12a)$$

where

$$\gamma = \left(sL_{\mathrm{e}}^2/D + \alpha^2/4\right)^{1/2}. \quad (12b)$$

When $U(x) = 0$, a condition realized by setting $\alpha = 0$, Eq. 12a reduces to the result given previously (20).

If the gating dynamics is slow on the timescales of the diffusional motion over the pore entrance cross section and down the pore, i.e., $\omega \ll D/a^2$ and D/L_e^2, it can be shown that Eq. 9 reduces to (33)

$$k_{\mathrm{e}+} \approx \frac{\omega_{\mathrm{o}}}{\omega}\, k_{\mathrm{se}+}. \quad (13)$$

Trp^{41} gating

In our model, the gating dynamics of Trp^{41} is coupled to the backbone dynamics of the transmembrane domain (11). Essentially, as far as binding to the internal site from the interior bulk solution is concerned, the transmembrane domain interconverts between two conformations. The open conformation allows for binding to the internal site, with the rate constant given by $k_{\mathrm{si}+}$ of Eq. 8b. In the other, the closed conformation, binding is prohibited. The ion flux for a channel that has an internal binding site and interconverts between two conformations has been derived (24). The result formally reduces to Eq. 1 when the conformational interconversion is much faster than proton binding/unbinding (see Appendix B), a condition that has been argued to apply to the M2 proton channel (20). The effective rate constant for proton binding to the internal site from the interior bulk solution is then given by

$$k_{\mathrm{i}+} = p_{\mathrm{open}}\, k_{\mathrm{si}+}, \quad (14)$$

where p_{open} is the equilibrium fraction of the open conformation.

Activation by low pH$_{\mathrm{e}}$

The M2 proton channel is activated by low pH$_{\mathrm{e}}$. Here, we assume that activation amounts to converting the closed conformation to the open conformation. We model activation explicitly by assuming that p_{open} depends on pH$_{\mathrm{e}}$; that is, p_{open} increases gradually as pH$_{\mathrm{e}}$ is lowered. In contrast to pH$_{\mathrm{e}}$, pH$_{\mathrm{i}}$ does not play any role in our modeling of channel activation, because, as we proposed previously (11), access to the His^{37} tetrad is blocked by the Trp^{41} gate until the C-terminal portion is already in the open conformation.

Model parameters

In our theory, we derive rate constants for proton binding from an explicit treatment of the structure and dynamics of the M2 channel. The results involve only a few well-characterized parameters. These include the proton diffusion constant D; the dissociation constant of the permeating proton, as measured by the third pK$_{\mathrm{a}}$, pK$_{\mathrm{a0}}$, of the His^{37} tetrad; four parameters determined by the structure of the M2 transmembrane domain (the full length of the pore L, the radius a and length L_{e} of the N-terminal pore, and the radius a_{i} of the C-terminal pore entrance in the open conformation); and three parameters determined by the dynamics of the M2 protein (transition rates ω_{c} and ω_{o} of the Val^{27} secondary gate and the equilibrium fraction p_{open} of the C-terminal open conformation). The value of D has been measured to be 10^3 Å^2/ns (22). The value of pK$_{\mathrm{a0}}$ has also been measured (18); here, pK$_{\mathrm{a0}}$ was fixed at 6. The structure of the M2 transmembrane domain (5–7) provides a solid basis for the geometric parameters of the pore; we set L, L_{e}, and a to be 35, 21, and 3 Å, respectively. Our choice of 5 Å for the value of a_{i} was guided by a model of the open conformation developed previously based on MD simulations (11). With these parameters, the binding rate constants $k_{\mathrm{se}+}$ and $k_{\mathrm{si}+}$ for a static pore have values of 0.7×10^9 and 1.7×10^9 M^{-1} s^{-1}, respectively, at $V = 0$ (see Eq. 5); values of 1.3×10^9 and 1.0×10^9 M^{-1} s^{-1}, respectively, at $V = -60$ mV; and values of 0.3×10^9 and 2.7×10^9 M^{-1} s^{-1}, respectively, at $V = 60$ mV (see Eq. 8).

There was less certainty on the three gating parameters, ω_{o}, ω_{c}, and p_{open}. We restricted these parameters to the following ranges: ω_{o} between 0.1 and 1 ns^{-1}; ω_{c} between 1 and 10 ns^{-1}; and p_{open} between 0.1 and 10%. These ranges were guided by MD simulations (9,11) and solid-state NMR experiments (8). The precise values of the three parameters were adjusted for each set of experimental data and are listed in the figure legends below. With these choices of parameters, the Val^{27} gating dynamics is close to the slow-gating limit: $k_{\mathrm{e}+}$ approaches the result given by Eq. 13. For example, at $\omega_{\mathrm{o}} = 0.1$ ns^{-1} and $\omega_{\mathrm{c}} = 1$ ns^{-1}, Eq. 9 predicts 10.3-, 9.7-, and 8.6-fold decreases from $k_{\mathrm{se}+}$ for $k_{\mathrm{e}+}$, at $V = -60$, 0, and 60 mV, respectively.

In comparison, Eq. 13 predicts an 11-fold decrease for all three voltages.

RESULTS

Here, we quantitatively test our theory against an extensive set of experimental data on M2 proton conductance. The experimental data of Chizhmakov et al. (12,16) were obtained from the whole-cell patch-clamp technique, which measured the total current conducted by multiple M2 proton channels, but the M2 copy numbers in the cells were unknown. (Only the currents due to M2 were used for the comparison here; that is, the rimantadine-resistant currents were subtracted from all the data.) In comparing against these experimental data, we scaled the calculated results for a single channel; the scaling factor was adjusted for optimal agreement. Chizhmakov et al. reported data for the M2 channels from two strains of influenza virus. Structural determinations and MD simulations have so far been restricted to the M2 of the Weybridge strain. Since our theory accounts for the structure and dynamics of the protein, in testing against the experiments of Chizhmakov et al. only the Weybridge conductance data were used. We further test our theory against the recent experimental data of Busath and coworkers (7). The latter data were obtained from M2 channels reconstituted into liposomes and report single-channel proton flux deduced from the known M2 copy number.

Current-voltage relations at fixed pH_e and pH_i

Chizhmakov et al. (12,16) measured current-voltage relations for a large number of interior and exterior pH values. All of these can be reproduced quite well by our theory. Fig. 2 shows the comparison of the experimental data with the calculation results. Consistent with our modeling of activation by pH_e, the values of p_{open} used for producing the results that match the experimental data increases with decreasing pH_e (see Fig. 2 legend). As Fig. 3 shows, the dependence of p_{open} on pH_e can be fitted to the function

$$p_{open} = p_{open\,0} e^{-(pH_e/pH_0)^5}, \qquad (15)$$

where $p_{open0} = 12.7\%$ and $pH_0 = 6.2$. It is interesting to note that the value of pH_0, which characterizes the transition of p_{open} from 0 at $pH_e \gg 1$ to the value p_{open0} at $pH_e = 0$, is close to the third pK_a value of the His^{37} tetrad.

pH_e-dependent proton flux at fixed pH_i and voltage

In Fig. 4 *A*, we show the dependence of the inward proton flux on pH_e when pH_i is fixed at 7.4. Two different voltages, −60 mV and +60 mV, are applied. Both sets of experimental data are well reproduced by the calculations. Chizhmakov et al. (12) presented their data as the chord

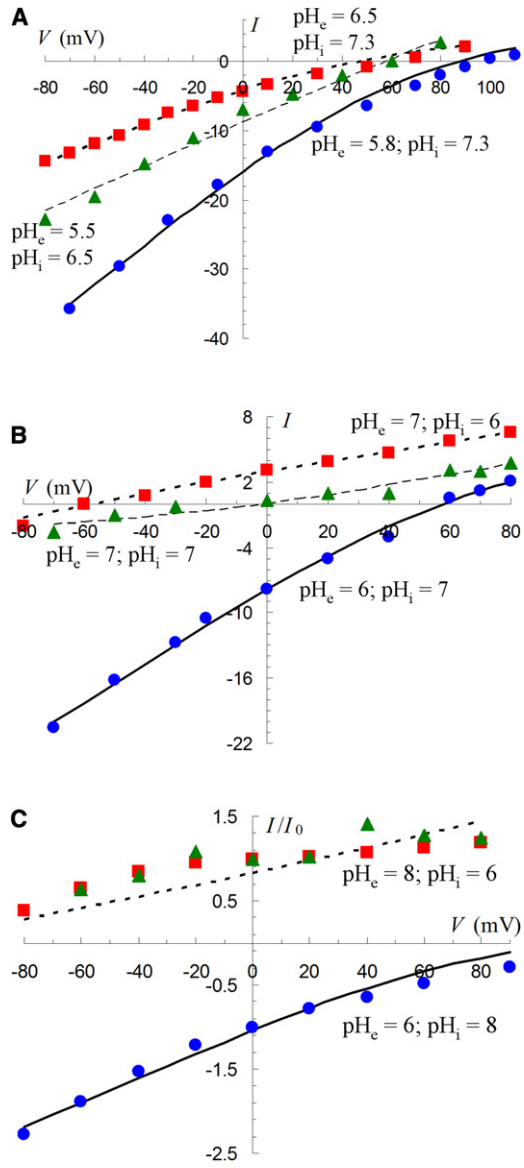

FIGURE 2 Current-voltage relations. (*A*) $pH_e = 5.8$ and 6.5, $pH_i = 7.3$; and $pH_e = 5.5$ and $pH_i = 6.5$. (*B*) $pH_e = 6$ and $pH_i = 7$; $pH_e = 7$ and $pH_i = 7$; and $pH_e = 7$ and $pH_i = 6$. (*C*) $pH_e = 6$ and $pH_i = 8$; and $pH_e = 8$ and $pH_i = 6$. Symbols display the experimental data of Chizhmakov et al. (12,16). The unit of I in *A* and *B* is immaterial, since the calculated results are scaled in comparing against the experimental data, which are shown in units of pA; the scaling corresponded to (1–5) × 10^6 functioning M2 channels/cell. In *C*, the data at $pH_e = 6$ and $pH_i = 8$ and one set of data at $pH_e = 8$ and $pH_i = 6$ were given as scaled by the respective currents at $V = 0$. The other set of data at $pH_e = 8$ and $pH_i = 6$ is similarly scaled here (after subtracting the rimantadine-resistant current). Curves are theoretical calculations. The values of ω_o and ω_c were set to 0.1 and 1 ns^{-1}, respectively, with the following exceptions: $\omega_o = 0.4$ ns^{-1} for $pH_e = 7$ and $pH_i = 6$ and for $pH_e = 8$ and $pH_i = 6$; $\omega_c = 3$ and 6 ns^{-1} for $pH_e = 6$ and $pH_i = 8$ and for $pH_e = 7$ and $pH_i = 7$, respectively. The values of p_{open} decreased with increasing pH_e: 7% for $pH_e = 5.5$; 6% for $pH_e = 5.8$; 5% for $pH_e = 6$; 4% for $pH_e = 6.5$; 2% for $pH_e = 7$ with $pH_i = 7$ and 1% for $pH_e = 7$ with $pH_i = 6$; and 0.1% for $pH_e = 8$.

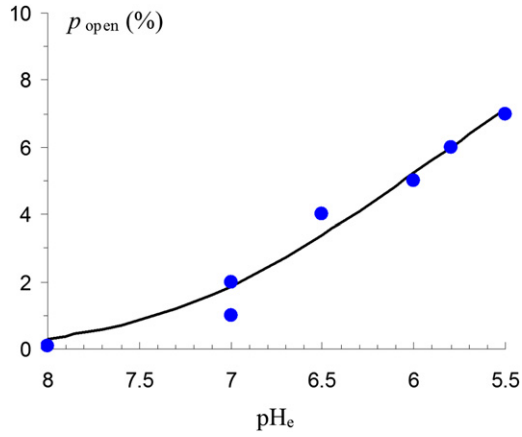

FIGURE 3 Fitting of the pH_e dependence of p_{open} to Eq. 15. Symbols are p_{open} values listed in the Fig. 2 legend; the curve is the fit to Eq. 15.

conductance, $g = I/(V - V_H)$, where V_H is the equilibrium potential, given by $58.4(pH_i - pH_e)$ mV. In our calculations, p_{open} was pH_e-dependent, as given by Eq. 15, to model activation by pH_e. If p_{open} were chosen to be independent of pH_e, the chord conductance would show a turnover at the low pH_e end. (In fact, even with a pH_e-dependent p_{open}, a slight turnover is discernible in the theoretical curve for $V = 60$ mV.) At fixed pH_i and V, whether p_{open} is independent of pH_e or has a pH_e dependence like Eq. 15, the inward proton flux monotonically increases when pH_e is lowered. However, the magnitude of $V - V_H$ also increases when pH_e is lowered. If p_{open} is independent of pH_e, the proton flux eventually saturates and lags behind the linearly increasing $|V - V_H|$, resulting in a turnover at low pH_e. That the experimental data do not show a turnover corroborates the assumption that p_{open} increases upon lowering p_{open}, which is our way of modeling activation by pH_e.

Fig. 4 *B* presents the dependence of the outward proton flux on pH_e when pH_i is fixed at 6.0 and the voltage is at 60 mV. Again, the experimental data (12) are well reproduced by the calculations. Note that here the dependence of the chord conductance on pH_e has a shape that is very different from that in Fig. 4 *A*. Our theory exquisitely captures both of the two different shapes.

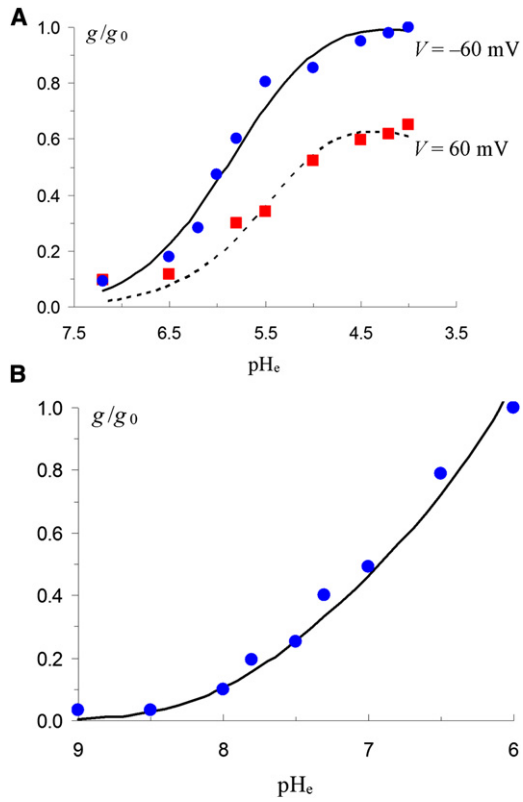

FIGURE 4 Dependence of proton flux on pH_e. (*A*) Inward flux, with pH_i fixed at 7.4 and $V = \pm 60$ mV. (*B*) Outward flux, with pH_i fixed at 6.0 and $V = 60$ mV. Symbols are the same as for the experimental data of Chizhmakov et al. (12). g_0 represents the chord conductance at $pH_i = 4.0$ and $V = -60$ mV in *A* and the chord conductance at $pH_i = 6.0$ and $V = 60$ mV in *B*. Curves are theoretical calculations. The values of the three gating parameters are $\omega_o = 0.2$ ns^{-1} and $\omega_c = 1$ ns^{-1} for *A* and $\omega_o = 0.1$ ns^{-1} and $\omega_c = 10$ ns^{-1} for *B*; and p_{open} as given by Eq. 15.

Single-channel proton flux

With M2 channels reconstituted into liposomes, it has become possible to deduce single-channel proton flux (7,14,19). A defining feature of M2 is its low proton flux, of the order of 100 protons/channel/s. Our theory predicts such low M2 proton flux. For example, for the case shown in Fig. 2 *A* with $pH_e = 5.8$ and $pH_i = 7.3$, the flux is 87 protons/channel/s at $V = -70$ mV.

Busath and co-workers (7) reported single-channel M2 proton fluxes for $pH_e = 6.5$, 6, and 5.5 while holding pH_i at 8 and V at –114 mV. Fig. 5 compares our predictions with the experimental data. The theory is in quantitative agreement with the experiment for all three pH_e values.

The results reported above are for a single set of geometrical parameters ($L = 35$ Å, $L_e = 21$ Å, $a = 3$ Å, and $a_i = 5$ Å). Very similar results are produced by our theory when these parameters are varied in physically reasonable

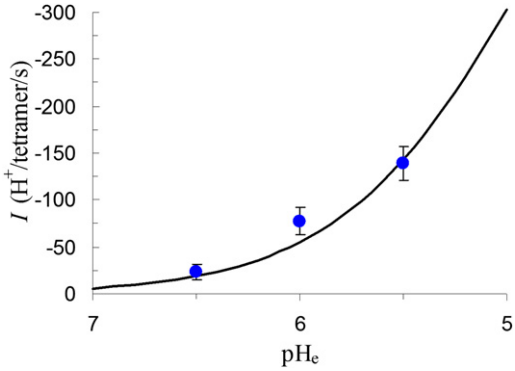

FIGURE 5 Comparison of calculated and experimental results for single-channel proton flux. The continuous curve displays our theoretical calculation with $\omega_o = 0.1$ ns^{-1} and $\omega_c = 2$ ns^{-1}; symbols show the data of Busath and co-workers (7).

ranges (e.g., $L \sim 25$–35 Å, $L_e/L \sim 0.6$, $a = 2.5$–3 Å, and $a_i/a = 1.5$–2). As for the dynamic parameters (ω_o, ω_c, and p_{open}), the results are qualitatively similar as long as ω_o and ω_c are in the nanosecond range and ω_o/ω_c and p_{open} are $\leq 10\%$.

DISCUSSION

We have shown that our microscopic theory, which incorporates the structural and dynamical properties of the M2 protein, is capable of quantitatively reproducing an extensive set of conductance data. Some of the same data have been fitted to a phenomenological model (yielding an expression for the proton flux analogous to Eq. 1), in which rate constants are introduced as fitting parameters (26). In contrast, we calculate the rate constants using theories of diffusion-influenced reactions. Our theory thus allows the proton-conductance function to be directly correlated with the structure and dynamics of the protein.

The physical (i.e., the proton diffusion constant), chemical (i.e., the dissociation constant of the permeant proton from the internal binding site), and geometrical parameters of our theory are well determined. There is somewhat less certainty on three dynamic parameters (ω_o, ω_c, and p_{open}) describing the gating of the channel, though even these parameters are tightly bound, based on previous MD simulations (9,11) and solid-state NMR experiments (8). Specifically, the simulations (9) showed that the Val^{27} gate at the entrance to the N-terminal pore is closed most of the time, and open-closed transitions occur on the nanosecond timescale. The constriction presented by the four Val^{27} residues is also observed in recent M2 structures (6,7), again indicating $\omega_o/\omega_c \ll 1$. A p_{open} value of $<10\%$, meaning that the C-terminal open conformation is a minor population, is supported by MD simulations (11) and the observation that peak positions of NMR spectra are unshifted when pH is lowered to a range where the channel becomes activated (8), though broadening of the peaks does suggest an increase in the population of the open conformation. Both the open-closed transitions of the Val^{27} gate and the interconversion of the C-terminal open and closed conformations are modeled as fast on the millisecond timescale. This aspect is supported by the observation that at both high and low pH, the NMR spectra of individual residues have single peaks, meaning that conformational averaging occurs fast on the NMR timescale (i.e., 1 ms). Furthermore, the time course of conductance induced by voltage change suggests "submillisecond 'gating' conformational changes" (16). It is important to note that with the tightly bound parameters, the theory produces the level of proton flux observed experimentally (7,14,19).

The results shown here seem to firmly establish the gating role of Val^{27}. Such a role was first proposed based on MD simulations (9); Val^{27} broke the water wire through the pore during most of the simulations. Our recent study (20) found that inclusion of Val^{27} gating brings the predicted proton flux to the same range as measured. Now we find that inclusion of Val^{27} gating allows our theory to quantitatively reproduce conductance measurements.

We account for channel activation by viral exterior pH, explicitly by modeling p_{open} as an increasing function as pH_e is lowered. Support is provided by the lack of a turnover of the chord conductance at low pH_e. As pH_e is lowered, an incoming proton in the N-terminal pore will likely interact with the His^{37} tetrad, thereby perhaps relieving the His^{37}-Trp^{41} interactions and opening the Trp^{41} gate. However, the detailed mechanism of how a change in pH_e is propagated to a change in the population of the open conformation is still a matter of speculation (6,7,34), and the derivation of a mathematical relation between p_{open} and pH_e like Eq. 15 remains to be investigated.

As noted above, a defining feature of M2 is its low proton flux, of the order of 10^2 protons/channel/s. In comparison, the transport rates of potassium and sodium channels are $>10^7$ ions/s. In our theory, the low level of M2 proton flux arises first from the permeant proton's obligatory binding to and unbinding from the internal site, i.e., the His^{37} tetrad. Moreover, the Trp^{41} primary gate and the Val^{27} secondary gate slow down the binding and unbinding. The role of Val^{27}, as discussed above, has been suggested by MD simulations and is supported by M2 structures (6,7). The roles of His^{37} and Trp^{41} in fact are suggested by experimental studies (4,15,17,18). That the theory, with physically reasonable parameters, quantitatively reproduces an extensive set of experimental conductance data provides support for the roles of these key residues in the M2 functional mechanism.

Chen et al. (35) carried out MD simulations (with a multistate empirical valence bond model accounting for proton-charge delocalization) to calculate the proton potential of mean force and the position-dependent diffusion constant. When the His^{37} tetrad was in the $+1$ charge state, a barrier was present around Val^{27}, which is perhaps consistent with its putative role as a secondary gate. For the $+3$ charge state of the His^{37} tetrad, the potential of mean force was relatively flat, except for a barrier between His^{37} and Trp^{41}. It is of interest that regardless of the protonation state of the His^{37} tetrad, the mean value of their position-dependent proton diffusion constant was $\sim 10^3$ Å^2/ns, which is the value used in our calculations. Chen et al. then modeled the proton transport as one-dimensional continuous electrodiffusion and applied the Poisson-Nernst-Planck theory to calculate the M2 proton conductance. They predicted a proton conductance of 53 pS for the $+3$ charge state of the His^{37} tetrad, which is equivalent to a proton flux of 3.3×10^7 protons/channel/s at $V = -100$ mV. This is 10-fold too high compared to an earlier measurement of Busath and co-workers (36) and five orders of magnitude too high compared to recent experimental data for single-channel proton conductance (7,14,19).

Our theory can be further tested. In particular, a change in solvent from H_2O to D_2O will affect the parameters in our theory in predictable ways. For example, the diffusion constant of the permeant ion, now a deuteron, will be reduced (22). Our predicted kinetic isotope effect can be tested by M2 currents measured in D_2O (13).

The basic framework of our theory allows for more realistic modeling of the structure and dynamics of the protein, through hybrid molecular dynamics and Brownian dynamics simulations. By Brownian dynamics simulations of the diffusive motion of the permeant proton and molecular dynamics simulations of the protein dynamics, we can calculate the binding rate constants with a more realistic representation of the protein (37). In the theory presented here, we have accounted for the potential of mean force arising from a transmembrane voltage, but neglected the potential of mean force that may arise from the interactions of the permeant proton with the protein and solvent environment. That the theory is able to reproduce well experimental results suggests that the latter type of potential of mean force either plays a negligible role in proton conductance or is mitigated by some other factor. The implementation of our theory by hybrid molecular dynamics and Brownian dynamics simulations will allow this and other detailed questions to be addressed.

APPENDIX A

Derivation of Eq. 12a

Here, we derive Eq. 12a for $\widehat{k}_{eP}(s)$, the Laplace transform of the total flux across the N-terminal pore entrance. The motion of ions in the pore is modeled as one-dimensional diffusion along the channel axis. We denote the product of the ion distribution function and the cross-sectional area as $p(x, t)$. It satisfies the diffusion equation (A. M. Berezhkovskii, A. Szabo, and H.-X. Zhou, unpublished)

$$\frac{\partial p(x,\,t)}{\partial t} = -\frac{\partial J(x,\,t)}{\partial x}, \tag{A1a}$$

$$J(x,\,t) = -De^{-U(x)/k_BT}\sigma(x)\frac{\partial}{\partial x}\left[e^{-U(x)/k_BT}\sigma(x)\right]^{-1}p(x,\,t). \tag{A1b}$$

In Eq. A1b, $U(x)$ is the potential of mean force resulting from averaging over the cross section at x, with a reference chosen such that $U(0) = 0$, and $J(x, t)$ is the total flux through the cross section at x.

The initial condition for $p(x, t)$ is

$$p(x,\,0) = 0. \tag{A2}$$

At the pore entrance, the boundary condition is

$$p(0,\,t) = \sigma(0). \tag{A3a}$$

We model binding to the internal site as diffusion-controlled, so that an absorbing boundary condition applies:

$$p(L_e,\,t) = 0. \tag{A3b}$$

The quantity we are looking for is

$$k_{eP}(t) = J(0,\,t). \tag{A3c}$$

In the case of a cylindrical pore with radius a and a linear potential $U(x)/k_BT = \alpha x/L_e$, Eq. A1 becomes

$$\frac{\partial p(x,\,t)}{\partial t} = D\frac{\partial^2 p(x,\,t)}{\partial x^2} + (D\alpha/L_e)\frac{\partial p(x,\,t)}{\partial x}. \tag{A4a}$$

The Laplace transform of this equation (with the use of the initial condition of Eq. A2) is

$$\frac{\partial^2 \widehat{p}(x,\,s)}{\partial x^2} + (\alpha/L_e)\frac{\partial \widehat{p}(x,s)}{\partial x} - (s/D)\widehat{p}(x,s) = 0. \tag{A4b}$$

The solution of the last equation can be written as

$$\widehat{p}(x,\,s) = A_1 e^{(-\alpha/2+\gamma)x/L_e} + A_2 e^{(-\alpha/2-\gamma)x/L_e}, \tag{A5}$$

where γ is given by Eq. 12b and A_1 and A_2 are coefficients to be determined by the boundary conditions of Eq. A3. The results of the coefficients are

$$A_1 = -\pi a^2/\left(e^{2\gamma}-1\right), \tag{A6a}$$

$$A_2 = \pi a^2 e^{2\gamma}/\left(e^{2\gamma}-1\right). \tag{A6b}$$

Calculating the flux at $x = 0$, we arrive at Eq. 12a.

We now briefly discuss two limiting cases. The first is when the potential is absent, and it is obtained by setting α to 0. Equation 12a then becomes

$$s\widehat{k}_{eP}(s) = \pi a^2 (sD)^{1/2}\coth\left(sL_e^2/D\right)^{1/2}. \tag{A7}$$

Using this expression in Eq. 9, we obtain the result for the rate constant for binding from the viral exterior under Val^{27} gating in the absence of a potential. This result was presented previously (20). Another limit is when $\omega \ll D/a^2$ and D/L_e^2. Applying the condition $s \ll D/a^2$ in Eq. 11, we find $s\widehat{k}_{eB}(s) \approx 4Da$, which is the inverse of the first term of Eq. 8a for k_{se+}. Applying the condition $s \ll D/L_e^2$ in Eq. 12a, we find $s\widehat{k}_{eP}(s) \approx \pi Da^2\alpha/L_e(e^\alpha - 1)$, which is the inverse of the second term of Eq. 8a for k_{se+}. Taken together, we find that when$\omega \ll D/a^2$ and D/L_e^2,

$$\frac{1}{\omega\widehat{k}_{eB}(\omega)} + \frac{1}{\omega\widehat{k}_{eP}(\omega)} \approx \frac{1}{4Da} + \frac{e^\alpha - 1}{\alpha}\frac{L_e}{\pi Da^2} = \frac{1}{k_{se+}}. \tag{A8}$$

Using this result in Eq. 9, we obtain the limiting expression for k_{e+} given by Eq. 13.

APPENDIX B

Derivation of Eq. 14

Here, we examine the case where the channel protein can interconvert between two conformations. The proton transport in each channel conformation is as described in the main text, but now the channel can switch its conformation while the permeant proton is still in the pore. If the conformational interconversion were fast on the timescale of the diffusional motion of the permeant ion through the pore, then the fluctuating channel could be modeled as having a static structure, with the potential of mean force given by the lifetime-weighted average over the two conformations. The diffusional time, D/L^2, is of the order of 1 ns; it is very likely that the conformational interconversion is slower. In that situation, in calculating the ion flux, we may use rate equations to describe the conformational interconversion.

We denote the two conformations as A and B and use a subscript 0 or 1 when the internal binding site is either unoccupied or occupied. There are four possible states: A_0, A_1, B_0, and B_1. Their interconversion can be described by the following scheme (24):

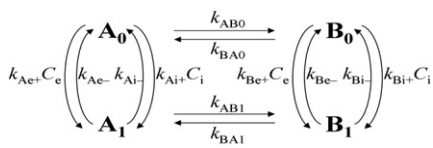

The vertical steps describe ion binding to and unbinding from the internal site; the rate constants k_{Ae+}, k_{Ae-}, etc. are the same as defined in the main text, but here they are specific to each conformation. The horizontal steps describe the conformational interconversion. The rate constants must satisfy detailed balance conditions

$$\frac{k_{AB1}/k_{BA1}}{k_{AB0}/k_{BA0}} = \frac{k_{Be+}/k_{Be-}}{k_{Ae+}/k_{Ae-}} = \frac{k_{Bi+}/k_{Bi-}}{k_{Ai+}/k_{Ai-}}. \tag{B1}$$

The ion flux can be calculated from the steady-state probabilities, q_{A0}, q_{A1}, q_{B0}, and q_{B1}, of the four states:

$$I = -k_{Ae+}C_e q_{A0} + k_{Ae-}q_{A1} - k_{Be+}C_e\, q_{B0} + k_{Be-}q_{B1}. \tag{B2}$$

The time dependence of the probability of each state is determined by a rate equation. For example, for state A_0, the rate equation is

$$\begin{aligned}\frac{dq_{A0}}{dt} &= -(k_{Ae+}C_e + k_{Ai+}C_i + k_{AB0})q_{A0} \\ &\quad + (k_{Ae-} + k_{Ai-})q_{A1} + k_{BA0}\, q_{B0}.\end{aligned} \tag{B3}$$

For the steady-state problem that we are interested in, each of these time derivatives is zero. In addition, the four steady-state probabilities sum to 1. Solving the algebraic equations for the steady-state probabilities, we find the ion flux to be

$$I = \frac{(-C_e + C_i/F)(k_{e+}k_{i-} + G)}{k_{e-} + k_{i-} + k_{e+}C_e + k_{i+}C_i + H}, \tag{B4}$$

where

$$k_{e+} = p_{A0}\,k_{Ae+} + p_{B0}\,k_{Be+}, \tag{B5a}$$

$$k_{i+} = p_{A0}\,k_{Ai+} + p_{B0}\,k_{Bi+}, \tag{B5b}$$

$$k_{e-} = p_{A1}k_{Ae-} + p_{B1}k_{Be-}, \tag{B5c}$$

$$k_{i-} = p_{A1}k_{Ai-} + p_{B1}k_{Bi-}, \tag{B5d}$$

$$F = \frac{k_{e+}/k_{e-}}{k_{i+}/k_{i-}} = \frac{k_{Ae+}/k_{Ae-}}{k_{Ai+}/k_{Ai-}} = \frac{k_{Be+}/k_{Be-}}{k_{Bi+}/k_{Bi-}}, \tag{B5e}$$

$$\begin{aligned}G &= p_{A0}(k_{i-}k_{Ae+}k_{Be+}C_e + Fk_{e-}k_{Ai+}k_{Bi+}C_i)/k_{BA0} \\ &\quad + p_{A1}(k_{e+}k_{Ai-}k_{Bi-} + Fk_{i+}k_{Ae-}k_{Be-})/k_{BA1},\end{aligned} \tag{B5f}$$

and

$$\begin{aligned}H &= p_{A0}(k_{A+}k_{B+} + p_{A1}k_{A-}k_{B+} + p_{B1}k_{A+}k_{B-})/k_{BA0} \\ &\quad + p_{A1}(k_{A-}k_{B-} + p_{A0}k_{A+}k_{B-} + p_{B0}k_{A-}k_{B+})/k_{BA1}.\end{aligned} \tag{B5g}$$

In Eq. B5, we have introduced the equilibrium fractions p_{A0} and p_{B0} of conformations A and B, respectively, in the unbound state, given by

$$p_{A0} = \frac{k_{BA0}}{k_{BA0} + k_{AB0}}; \tag{B6a}$$

$$p_{B0} = \frac{k_{AB0}}{k_{BA0} + k_{AB0}} = 1 - p_{A0}. \tag{B6b}$$

In a similar way, the equilibrium fractions p_{A1} and p_{B1} of conformations A and B, respectively, in the bound state are given by

$$p_{A1} = \frac{k_{BA1}}{k_{BA1} + k_{AB1}}; \tag{B6c}$$

$$p_{B1} = \frac{k_{AB1}}{k_{BA1} + k_{AB1}} = 1 - p_{A1}. \tag{B6d}$$

The additional quantities $k_{A\pm}$ in Eq. B5g are given by

$$k_{A+} = k_{Ae+}C_e + k_{Ai+}C_i; \tag{B7a}$$

$$k_{A-} = k_{Ae-} + k_{Ai-}; \tag{B7b}$$

and analogously for $k_{B\pm}$.

When the conformational interconversion is fast on the timescale of ion binding and unbinding, i.e., when the first-order rate constants for the horizontal steps are much greater than the (pseudo) first-order rate constants for the vertical steps, G and $H \to 0$, and Eq. B4 reduces to Eq. 1. The effective binding and unbinding rate constants are given by Eq. B5a–d. Specializing to our modeling of the C-terminal gating in the M2 proton channel, A and B represent the open and closed conformations, respectively. In the closed conformation, binding to the internal site from the viral interior is prohibited, i.e., $k_{Bi+} = 0$. Equation B5b then reduces to Eq. 14 once p_{A0} is identified with p_{open}, the equilibrium fraction of the open conformation, and k_{Ai+} is identified with k_{si+}, the rate constant for binding from the viral interior when the channel stays in the open conformation.

I thank Hao Dong for digitizing the experimental data from the works by Chizhmakov and colleagues (12,16), which are used here to test the theory.

This work was supported in part by National Institutes of Health grants GM58187 and AI23007.

REFERENCES

1. Sugrue, R. J., and A. J. Hay. 1991. Structural characteristics of the M2 protein of influenza A viruses: evidence that it forms a tetrameric channel. *Virology.* 180:617–624.
2. Pinto, L. H., L. J. Holsinger, and R. A. Lamb. 1992. Influenza virus M2 protein has ion channel activity. *Cell.* 69:517–528.
3. Takeda, M., A. Pekosz, …, R. A. Lamb. 2002. Influenza a virus M2 ion channel activity is essential for efficient replication in tissue culture. *J. Virol.* 76:1391–1399.
4. Pinto, L. H., G. R. Dieckmann, …, W. F. DeGrado. 1997. A functionally defined model for the M2 proton channel of influenza A virus suggests a mechanism for its ion selectivity. *Proc. Natl. Acad. Sci. USA.* 94:11301–11306.
5. Nishimura, K., S. Kim, …, T. A. Cross. 2002. The closed state of a H^+ channel helical bundle combining precise orientational and distance restraints from solid state NMR. *Biochemistry.* 41:13170–13177.
6. Acharya, R., V. Carnevale, …, M. L. Klein. 2010. Structure and mechanism of proton transport through the transmembrane tetrameric M2 protein bundle of the influenza A virus. *Proc. Natl. Acad. Sci. USA.* 107:15075–15080.

7. Sharma, M., M. Yi, …, T. A. Cross. 2010. Insight into the mechanism of the influenza A proton channel from a structure in a lipid bilayer. *Science.* 330:509–512.
8. Li, C., H. Qin, …, T. A. Cross. 2007. Solid-state NMR characterization of conformational plasticity within the transmembrane domain of the influenza A M2 proton channel. *Biochim. Biophys. Acta.* 1768:3162–3170.
9. Yi, M., T. A. Cross, and H.-X. Zhou. 2008. A secondary gate as a mechanism for inhibition of the M2 proton channel by amantadine. *J. Phys. Chem. B.* 112:7977–7979.
10. Khurana, E., M. Dal Peraro, …, M. L. Klein. 2009. Molecular dynamics calculations suggest a conduction mechanism for the M2 proton channel from influenza A virus. *Proc. Natl. Acad. Sci. USA.* 106:1069–1074.
11. Yi, M., T. A. Cross, and H.-X. Zhou. 2009. Conformational heterogeneity of the M2 proton channel and a structural model for channel activation. *Proc. Natl. Acad. Sci. USA.* 106:13311–13316.
12. Chizhmakov, I. V., F. M. Geraghty, …, A. J. Hay. 1996. Selective proton permeability and pH regulation of the influenza virus M2 channel expressed in mouse erythroleukaemia cells. *J. Physiol.* 494:329–336.
13. Mould, J. A., H.-C. Li, …, L. H. Pinto. 2000. Mechanism for proton conduction of the M(2) ion channel of influenza A virus. *J. Biol. Chem.* 275:8592–8599.
14. Lin, T. I., and C. Schroeder. 2001. Definitive assignment of proton selectivity and attoampere unitary current to the M2 ion channel protein of influenza A virus. *J. Virol.* 75:3647–3656.
15. Tang, Y., F. Zaitseva, …, L. H. Pinto. 2002. The gate of the influenza virus M2 proton channel is formed by a single tryptophan residue. *J. Biol. Chem.* 277:39880–39886.
16. Chizhmakov, I. V., D. C. Ogden, …, A. J. Hay. 2003. Differences in conductance of M2 proton channels of two influenza viruses at low and high pH. *J. Physiol.* 546:427–438.
17. Venkataraman, P., R. A. Lamb, and L. H. Pinto. 2005. Chemical rescue of histidine selectivity filter mutants of the M2 ion channel of influenza A virus. *J. Biol. Chem.* 280:21463–21472.
18. Hu, J., R. Fu, …, T. A. Cross. 2006. Histidines, heart of the hydrogen ion channel from influenza A virus: toward an understanding of conductance and proton selectivity. *Proc. Natl. Acad. Sci. USA.* 103:6865–6870.
19. Leiding, T., J. Wang, …, S. P. Arsköld. 2010. Proton and cation transport activity of the M2 proton channel from influenza A virus. *Proc. Natl. Acad. Sci. USA.* 107:15409–15414.
20. Zhou, H.-X. 2010. Diffusion-influenced transport of ions across a transmembrane channel with an internal binding site. *J. Phys. Chem. Lett.* 1:1973–1976.
21. Swanson, J. M., C. M. Maupin, …, G. A. Voth. 2007. Proton solvation and transport in aqueous and biomolecular systems: insights from computer simulations. *J. Phys. Chem. B.* 111:4300–4314.
22. Roberts, N. K., and H. L. Northey. 1974. Proton and deuteron mobility in normal and heavy water solutions of electrolytes. *J. Chem. Soc., Faraday Trans. I.* 70:253–262.
23. Eigen, M., and G. G. Hammes. 1963. Elementary steps in enzyme reactions (as studied by relaxation spectrometry). *Adv. Enzymol. Relat. Areas Mol. Biol.* 25:1–38.
24. Läuger, P. 1985. Ionic channels with conformational substates. *Biophys. J.* 47:581–590.
25. Levitt, D. G. 1986. Interpretation of biological ion channel flux data—reaction-rate versus continuum theory. *Annu. Rev. Biophys. Biophys. Chem.* 15:29–57.
26. Lear, J. D. 2003. Proton conduction through the M2 protein of the influenza A virus; a quantitative, mechanistic analysis of experimental data. *FEBS Lett.* 552:17–22.
27. Miloshevsky, G. V., and P. C. Jordan. 2004. Permeation in ion channels: the interplay of structure and theory. *Trends Neurosci.* 27:308–314.
28. Bolintineanu, D. S., A. Sayyed-Ahmad, …, Y. N. Kaznessis. 2009. Poisson-Nernst-Planck models of nonequilibrium ion electrodiffusion through a protegrin transmembrane pore. *PLOS Comput. Biol.* 5:e1000277.
29. Jordan, P. C., R. J. Bacquet, …, P. Tran. 1989. How electrolyte shielding influences the electrical potential in transmembrane ion channels. *Biophys. J.* 55:1041–1052.
30. Roux, B. 1999. Statistical mechanical equilibrium theory of selective ion channels. *Biophys. J.* 77:139–153.
31. Zhou, H.-X. 1998. Theory of the diffusion-influenced substrate binding rate to a buried and gated active site. *J. Chem. Phys.* 108:8146–8154.
32. Zwanzig, R., and A. Szabo. 1991. Time dependent rate of diffusion-influenced ligand binding to receptors on cell surfaces. *Biophys. J.* 60:671–678.
33. Zhou, H.-X. 2010. Rate theories for biologists. *Q. Rev. Biophys.* 43:219–293.
34. Hu, F., W. Luo, and M. Hong. 2010. Mechanisms of proton conduction and gating in influenza M2 proton channels from solid-state NMR. *Science.* 330:505–508.
35. Chen, H., Y. Wu, and G. A. Voth. 2007. Proton transport behavior through the influenza A M2 channel: insights from molecular simulation. *Biophys. J.* 93:3470–3479.
36. Vijayvergiya, V., R. Wilson, …, D. D. Busath. 2004. Proton conductance of influenza virus M2 protein in planar lipid bilayers. *Biophys. J.* 87:1697–1704.
37. Zhou, H.-X., S. T. Wlodek, and J. A. McCammon. 1998. Conformation gating as a mechanism for enzyme specificity. *Proc. Natl. Acad. Sci. USA.* 95:9280–9283.